Photodiagnosis and Photodynamic Therapy 27 (2019) 305–316

Contents lists available at ScienceDirect

Photodiagnosis and Photodynamic Therapy

journal homepage: www.elsevier.com/locate/pdpdt

Antimicrobial photodynamic activity of toluidine blue-carbon nanotube conjugate against *Pseudomonas aeruginosa* and *Staphylococcus aureus* - Understanding the mechanism of action

V.T Anju[a], Parasuraman Paramanantham[a], Sruthil Lal S.B[b], Alok Sharan[b], Asad Syed[c], Needa A. Bahkali[d], Marzouq H. Alsaedi[c], K. Kaviyarasu[e,f,**], Siddhardha Busi[a,*]

[a] Department of Microbiology, School of Life Sciences, Pondicherry University, Puducherry, 605014, India
[b] Department of Physics, School of Physical, Chemical &amp, Applied Sciences, Pondicherry University, Puducherry, 605014, India
[c] Department of Botany and Microbiology, College of Science, King Saud University, Riyadh, 11451, Saudi Arabia
[d] Biological Sciences Department, Wagner College, 1 Campus Rd, Staten Island, NY, 10301, USA
[e] UNESCO-UNISA Africa Chair in Nanoscience's/Nanotechnology Laboratories, College of Graduate Studies, University of South Africa (UNISA), Muckleneuk Ridge, P O Box 392, Pretoria, South Africa
[f] Nanosciences African Network (NANOAFNET), Materials Research Group (MRG), iThemba LABS-National Research Foundation (NRF), 1 Old Faure Road, 7129, P O Box 722, Somerset West, Western Cape Province, South Africa

ARTICLE INFO

Keywords:
Antimicrobial photodynamic therapy
Planktonic cells
Toluidine blue multiwalled carbon nanotube
Reactive oxygen species
Pseudomonas aeruginosa
Staphylococcus aureus

ABSTRACT

Background: The emergence of drug-resistant bacterial strains has raised the need to develop alternative treatment modalities to combat infectious diseases. Antimicrobial photodynamic therapy (aPDT) is an alternative to conventional treatment modalities. aPDT integrates a photosensitizer, which, after exposure to light of an appropriate wavelength, leads to the generation of cytotoxic reactive oxygen species (ROS).
Methods: The aim of the present study was to synthesize a toluidine blue/multiwalled carbon nanotube conjugate (TBCNT) for enhanced photoinactivation of *Pseudomonas aeruginosa* and *Staphylococcus aureus*. Synthesized TBCNT conjugate was characterized and its antibacterial and antibiofilm activity was determined.
Results: During TBCNT synthesis, dye loading, and entrapment efficiency of the CNT were 12.04 ± 0.55% and 48.99 ± 2.33%, respectively. The photo-destruction of planktonic cells of the test bacteria was performed by exposure to a 125 mW red laser with a wavelength of 670 nm (radiant exposure of 58.49 J/cm^2) for 3 min. Photoinactivation using TBCNT resulted in a 4.91- and 5.47-log10 reduction in *P. aeruginosa* and *S. aureus*, respectively. The mechanism of this aPDT was studied by measuring intracellular ROS generation, protein leakage, and lipid peroxidation in the test bacteria after light irradiation. The antibiofilm activity of TBCNT after light exposure was 69.94% and 75.54% for *P. aeruginosa* and *S. aureus*, respectively. Photoinactivation of test bacteria treated with TBCNT reduced cell viability and exopolysaccharide production. Confocal laser-scanning microscopy revealed a significant biofilm inhibition efficacy of the TBCNT conjugate.
Conclusion: Therefore, TBCNT conjugates may be used for the eradication of *P. aeruginosa* and *S. aureus* biofilms.

1. Introduction

The emergence of antibiotic resistant microorganism has led to the development of serious health problems in recent years. Most of the infectious pathogens are resistant to at least one of the existing antimicrobial agents, which are generally employed to eliminate the pathogens. The global threat of antibiotic resistance is associated with higher health care costs [1]. Report says that world will loss 10 million lives by the end of 2050 due to the emerging resistant bacterial strains. This emerging threat forced the researchers to find alternative solutions to eliminate these bacterial strains [2]. This global health threat owing to the antimicrobial resistance urged the need to discover alternatives. AMR bacteria are difficult to treat by conventional antimicrobial agents [3]. Origin and molecular mechanism of antibiotic resistance are diverse and complex process in every bacterium. The evolution of new mechanisms of resistance has resulted in the emergence of several

* Corresponding author.
** Corresponding author at: UNESCO-UNISA Africa Chair in Nanoscience's/Nanotechnology Laboratories, College of Graduate Studies, University of South Africa (UNISA), Muckleneuk Ridge, P O Box 392, Pretoria, South Africa.
E-mail addresses: kaviyarasuloyolacollege@gmail.com (K. K.), Siddhardha.busi@gmail.com (S. Busi).

https://doi.org/10.1016/j.pdpdt.2019.06.014
Received 3 April 2019; Received in revised form 9 May 2019; Accepted 17 June 2019
Available online 20 June 2019
1572-1000/

dangerous resistant strains including multidrug-resistant (MDR) bacterial strains, known as '*superbugs*' [4]. These superbugs are able to produce antibiotic resistant biofilms. Antibiotic resistance in microbial biofilms is mainly contributed by their life style. Biofilms constitute cells which coordinate among themselves that are encased in a self-protective polymeric matrix or exopolysaccharides. Biofilms are responsible for chronic infections by colonizing the prosthetic devices such as indwelling catheters and endotracheal tubes [5].

Antimicrobial photodynamic therapy is an emerging non- antibiotic approach for the elimination of antibiotic resistant microorganisms [6]. aPDT employs a nontoxic dye or photosensitizer and low intensity light which produces cytotoxic oxygen species in presence of molecular oxygen. The antimicrobial effect is due to the generation of free radicals that results from the PS exposed to light [7]. The lethal damage to the cell includes cellular damage, membrane lysis, protein inactivation and DNA damage [8]. aPDT is proficient in inactivation of all known classes of microorganisms such as bacteria, fungi, protozoa and viruses. The major limitations of a PS in aPDT are poor solubility and the tendency to aggregate in aqueous solution forming dimers, trimers etc. Nanocarriers can be employed to overcome these limitations.

Nanotechnology is a promising strategy to prevent biofilms with diverse mode of antibiofilm mechanisms compared to the traditional antimicrobials [9]. Nanotechnology has created new windows in the antibiofilm research as the nanomaterials are highly efficient in penetrating the biofilm matrix [10]. Various metal nanoparticles are studied due to their antimicrobial and photocatalytic properties [11,12]. Green synthesized nickel oxide nanoparticles were removed organic dyes due to their photocatalytic degradation property [13]. Some nanoparticles act as drug carriers and as well as antimicrobial agents. In a study, authors reported antimicrobial activity of zinc oxide-copper oxide nanocomposites against *P. aeruginosa* and *S. aureus* [14]. The nanocarriers has contributed promising results in aPDT by increasing the solubility and delivery of hydrophobic PS [15]. Recent reports had emphasized on carbon encapsulated materials including carbon nanotubes, fullerenes, graphene oxide etc as drug delivery agents and also known for their antibacterial activities [16]. Carbon nanotubes are innovative nanomaterial with novel physiochemical, mechanical, antimicrobial and electrical properties [17]. The excellent properties of carbon nanotubes (CNT) makes them appropriate in different applications such as super capacitors, as biosensors, for drug delivery, in tissue engineering and antimicrobial photothermal therapy [18]. CNTs are excellent drug carriers due to their outstanding properties such as tunable morphology that provides biocompatibility and enhanced solubility [19].

Among a great number of photosensitizers available and studied, Phenothiazinium family of dyes are widely used in antimicrobial photoinactivation. These are efficient photosensitizers having increased binding and permeability to both Gram positive and Gram negative bacteria [20]. The previous reports on antimicrobial photodynamic therapy clearly suggests the broad spectrum antimicrobial action of various cationic and anionic dyes [21]. Toluidine blue is an cationic photosensitizer exhibiting phototoxicity against broad spectrum microorganisms. In a study, toluidine blue conjugated silver nanoparticles were used for the photodynamic inactivation of *Streptococcus mutants* biofilms [22]. Toluidine blue (TB) was reported as an effective photosensitizer against biofilms of *P. aeruginosa* and *S. aureus* [23]. Although the photo bactericidal activity of TB was studied *in vitro*, the poor solubility and tendency to form ineffective aggregates demands the synthesis of nanoconjugates. The present work is focused to evaluate the effective and enhanced photodynamic inactivation of *P. aeruginosa* and *S. aureus* biofilms using toluidine blue conjugated carbon nanotubes.

2. Materials and methods

2.1. Chemicals, bacterial strains and growth media

Carboxyl functionalized multiwalled carbon nanotubes with a length and diameter of 1.5 μm and 9.5 nm were purchased from Sigma-Aldrich, USA. Toluidine blue (TB), Luria Bertani broth (LB) and Agar were procured from Hi-Media, India. Bacteria used in this study were *Pseudomonas aeruginosa* PA01 and *Staphylococcus aureus* MCC 2408. *P. aeruginosa* PA01, a standard biofilm producing bacterium, was gifted by Prof. E. Peter Greenberg (Department of Microbiology, University of Washington and School of Medicine). *S. aureus* MCC 2408 was obtained from Microbial Culture Collection (MCC), National Centre for Microbial Resource, Pune, India. The bacteria were cultured in Luria Bertani (LB) broth in aerobic conditions at 37 °C in a shaker incubator. An overnight bacterial culture of 0.5 McFarland standard containing 1.5×10^8 CFU/mL was used for all *in vitro* assays.

2.2. Synthesis of TBCNT conjugate

Briefly, 5 mg of carboxyl functionalized CNT dispersed in double distilled water (10 mL) and mixed with toluidine blue dye (0.25 mg). The solution was magnetically stirred for 1 h at room temperature. The reaction mixture was sonicated for 15 min at room temperature and subjected to continuous magnetic stirring for 24 h. The mixture was centrifuged and washed thrice with deionized water. The bluish black pellet obtained was collected and dried. The dried powder was used for characterization and biological studies [24].

2.3. Characterization of TBCNT conjugate

Optical properties of TBCNT was recorded using a UV-VIS-NIR spectrophotometer (varian model: 5000) in the wavelength range of 250–800 nm. High resolution transmission electron micrograph (HRTEM) of TBCNT was obtained from HITACHI H-8100 electron microscopy (Hitachi, Tokyo, Japan) operated with an accelerating voltage of 20 KV. FTIR spectrum of CNT, TB and TBCNT conjugate was graphed using a Fourier transform infrared spectrometer (thermo nicolet model: 6700). The FTIR spectra was recorded and identified in a wavelength range of 400–4000 cm^{-1} with resolution of 0.1 cm^{-1}. The Raman spectrum of TBCNT was obtained by Raman Renishaw spectrometer with an excitation laser of 785 nm. The vibrational modes formed in the Raman spectra resulted from scattering of photons was recorded using Raman spectroscopy. Photo excitation and emission spectra of CNT, TB and TBCNT were studied using Fluorescence spectrophotometer (make: Jobin Yvon, model: FLUOROLOG -FL3-11) equipped with a xenon lamp as the excited light source at room temperature (0.2 nm resolution).

2.4. Loading capacity of dye and entrapment efficiency of CNT

The loading capacity (LC) and entrapment efficiency (EE) were measured according to the previous report with slight modifications [25]. Two milligrams of TBCNT conjugate was dispersed in 2 mL of absolute ethanol and vortexed for 5 min. The solution was centrifuged at 10000 rpm for 10 min which enables the complete release of dye from TBCNT. The supernatant obtained was measured spectrophotometrically at 630 nm to calculate the amount of TB loaded onto the CNTs. The percentage of LC and EE were calculated using the formula;

$$\text{Dye Loading capacity} = [M_1/ M_2] \times 100$$

$$\text{Entrapment efficiency} = [M_1/ M_3] \times 100$$

Where M_1 is the weight of TB in TBCNT, M_2 is the weight of CNT used, M_3 is the total weight of TB used for conjugation experiment.

2.5. Dye release study

The dye release study was performed according to the method described elsewhere with slight modifications [26]. To obtain the release profile of TB from TBCNT, dye loaded CNT (1 mg) was dispersed in 1 mL of PBS at 37 °C (pH = 7.4) and kept in shaking conditions (125 rpm) for 3 h. At different time intervals (every 30 min) aliquots of reaction mixture was collected and centrifuged at 10000 rpm for 10 min to test the amount of dye released. One milliliter of PBS was added to the tube after taking out the supernatant for UV absorbance at 630 nm. Release profile of TB was recorded by measuring the optical density of supernatant at 630 nm.

2.6. Bacterial uptake of TB

The bacterial uptake of TB from the cells treated with free TB and TBCNT was analyzed using the method described previously [27]. Overnight cultures of bacteria were centrifuged and OD was adjusted to 1.5×10^8 CFU/mL. About 2 mL of culture was incubated with 2 mg of TBCNT and free TB in dark for different time intervals (30, 60, 90, 120, 150 and 180 min) on a shaking incubator (125 rpm). The solution was centrifuged at 10000 rpm for 10 min. The obtained pellet was washed gently using PBS to remove the unbound TB. Cell bound TB was extracted by incubating with methanol (1 mL) at room temperature for 1 h. The mixture was again centrifuged at 10000 rpm for 10 min and the TB present in the supernatant solution spectrophotometrically measured at 630 nm. The amount of TB internalized by bacteria was determined using the equation;

% Uptake of TB = [Amount of TB in the dissolved pellet / Total amount of TB added] × 100

2.7. Photosensitizer and light source

Toluidine blue (TB) was used as the photosensitizer. A stock solution of 10 mg/mL of TB was prepared and stored in dark. The samples were photoactivated using a 125 mW red diode laser with emission wavelength of 670 nm. The photoinactivation of samples were carried out in a 96- well microtitre plate with flat bottom wells having circular shape. The area of irradiation was calculated as πr^2 (r; radius of well, 0.35 cm).

The radiant exposure was calculated as follows:

Radiant exposure = P.D × Exposure time.

Power density (P.D) = P (W)/ A (cm^2)

(P; the output power of laser used for exposure in Watts (W) and A; the irradiated area in cm^2 (πr^2)) [28].

The radiant exposure of laser was calculated according to the average output power and time of irradiation of samples. The bacteria were treated with TB (50 μg/mL) and TBCNT (416.6 μg/mL) with a final concentration of TB equal to 50 μg/mL. Concentration of CNT (366.6 μg/mL) was fixed according to the concentration of CNT present in the TBCNT. All the test samples were light irradiated for 3 min after the pre-incubation in dark for 3 h. Spectral parameters used in this study were given in the Table 1.

The test samples were distributed as 8 different groups.

Sample 1- Control (L^-); Bacterial samples incubated in dark and not treated with CNT, TB and TBCNT.

Sample 2- Control (L^+); Bacterial samples irradiated in the absence CNT, TB and TBCNT.

Sample 3- CNT (L^-); Bacterial samples treated with CNT and not irradiated.

Sample 4- CNT (L^+); Bacterial samples treated with CNT and irradiated.

Sample 5- TB (L^-); Bacterial samples treated with TB and not irradiated

Sample 6- TB (L^+); Bacterial samples treated with TB and irradiated

Sample 7- TBCNT (L^-); Bacterial samples treated with TBCNT and not irradiated

Sample 8- TBCNT (L^+); Bacterial samples treated with TBCNT and irradiated

Table 1
Spectral calculations and experimental parameters used in antimicrobial photodynamic inactivation studies.

Diode LASER	670 nm
Peak wavelength (nm)	630 nm
Operation mode	Continuous mode
Radiant power (mW)	125
Polarization	Random
Exposure duration (min)	3
Radiant exposure (J/cm^2)	58.49
Irradiated area (cm^2)	0.385
Application technique	Top irradiation
Number of treatments	1

2.8. Photodynamic inactivation of bacteria

Antimicrobial photodynamic inactivation of planktonic cells of test bacteria using TBCNT conjugate was studied [29]. Overnight test cultures were diluted to a concentration of 0.5 McFarland standard (1.5×10^8 CFU/mL) and aliquots of 100 μL of culture was transferred into the 96 well plate. All the eight test sample groups were maintained in 96 well plates with appropriate labels. All the samples were treated with CNT, TB and TBCNT conjugate at their specific concentration of 366.6, 50 and 416.6 μg/mL respectively. All the samples were incubated in dark for 3 h prior to the irradiation. Sample 2, 4, 6 and 8 were light irradiated using a red laser of 670 nm for 3 min with a radiant exposure of 58.49 J/cm^2. Samples 1, 3, 5 and 7 were kept in dark conditions. Samples treated with and without light were diluted serially in multitier plate containing 100 μL of LB broth. After incubation for 24 h at 37 °C, the number of colonies were counted. The obtained results were expressed as the logarithmic reduction in the planktonic cells by comparing with the control (CFU/mL).

2.9. Study of mechanism of action

2.9.1. Detection of reactive oxygen species (ROS)

The ROS produced after aPDT was detected using 2′,7′- dichlorofluorescein diacetate (DCFH-DA) [30]. The overnight test culture (1.5×10^8 CFU/mL) was treated with CNT, TB and TBCNT in appropriate concentration and pre-incubated for 3 h. The pre-incubated samples were treated with 5 mM DCFH-DA and incubated in dark for 10 min. Excess of DCFH-DA from the samples was removed by centrifugation and irradiated for 3 min. The control wells were maintained untreated. A similar experiment was maintained in dark for comparison. The fluorescent intensity produced was measured using fluorescence spectroscopy at an excitation wavelength of 485 nm.

2.9.2. Analysis of cytoplasmic leakage

The effect of aPDT on the integrity of bacterial cell membrane was analyzed through the release of intracellular biomolecules. The cytoplasmic leakage of protein was determined by using standard Bradford's protein estimation method [31]. A positive control was maintained by treating the sample with 10 μg/mL of CTAB (Cetyl Trimethyl Ammonium Bromide) to obtain cytoplasmic leakage index. The test bacteria were treated with CNT, TB and TBCNT. The samples were pre-incubated in dark for 3 h and irradiated for 3 min. The samples treated with and without light were centrifuged at 10,000 rpm for 5 min to remove the bacterial cells. The absorbance of supernatant was recorded at 595 nm to determine the amount of protein leaked. The protein

leakage of treated samples was calculated by comparing with the results of CTAB treated samples.

2.9.3. Lipid peroxidation assay

Thiobarbituric acid reactive substances (TBARS) assay was performed for the detection of membrane lipid peroxidation [32]. Lipid peroxidation will occur in test bacteria due to the oxidative stress mediated by light irradiation. This results in the formation of complex and reactive compounds such as 4-hydroxynonenal (4-HNE) and malondialdehyde (MDA). The produced MDA was measured using TBARS assay. Cellular damage in aPDT treated cells leads to the formation of lipid peroxides. The test cultures (1.5×10^8 CFU/mL) were treated with CNT, TB and TBCNT and pre-incubated in dark for 3 h. After pre-incubation, one set of samples including a control was irradiated with light of 670 nm. A similar experiment was conducted for the samples treated with CNT, TB and TBCNT and incubated in dark. All samples were mixed with 10% ice-cold TCA. The samples were centrifuged at 14000 rpm for 15 s and the homogenate formed was collected. One milliliter of supernatant was mixed with 1 mL of 0.6% 2-Thiobarbituric acid (TBA) and heated in boiling water for 10 min. The samples were cooled to room temperature and the chromogenic complex formed was detected spectrophotometrically at 535 nm. The lipid peroxides formation was quantified by comparing with the MDA standards.

2.10. Antibiofilm activity

2.10.1. Biofilm inhibition assay

Biofilm inhibition assay was performed using the method described previously with slight modifications [22]. Overnight culture of test bacteria were diluted to 1.5×10^8 CFU/mL and incubated with CNT, TB and TBCNT conjugate. The samples were pre-incubated for 3 h and irradiated for 3 min. A set of samples were irradiated with laser and other was kept in dark. A control well with culture broth and bacteria was maintained in both the experimental setup. All samples were diluted in LB broth and incubated at 37 °C for 24 h. After incubation, the wells were washed gently with PBS in order to remove planktonic bacteria. The wells were allowed to air dry and stained with 200 µL of 0.1% crystal violet at room temperature for 15 min. The wells were slightly washed with PBS and cell bound crystal violet was eluted with 100 µL of 95% ethanol. The biofilm inhibition was quantified spectrophotometrically at OD_{590} by measuring the absorption of the eluted dye. Inhibition in the biofilm formation was calculated by using the following formula:

% of Inhibition = [(OD_{590} in control – OD_{590} of test) / OD_{590} in control] × 100

2.10.2. Cell viability assay

Cell viability after aPDT was analyzed using 2,3,5-Triphenyltetrazolium chloride (TTC) assay [33]. Overnight cultures were adjusted to a McFarland standard containing 1.5×10^8 CFU/mL of test bacteria and treated with appropriate concentrations of CNT, TB and TBCNT. The wells with culture broth and bacteria were served as control. All the samples were pre incubated in dark for 3 h and irradiated for 3 min using a light of 670 nm wavelength. All the samples were serially diluted in Luria Bertani broth (100 µL) and kept for incubation at 37 °C for 24 h. After incubation, the wells were rinsed with sterile PBS and to the each well, 100 µL of 0.5% freshly prepared TTC was added. A similar experiment was conducted and incubated in dark for comparison. The plates were incubated for 5 min at room temperature and the absorbance was measured spectrophotometrically at 485 nm.

2.10.3. Exopolysaccharides (EPS) quantification assay

Exopolysaccharides was quantified using the congo red (CR) agar method [34]. A standard suspension of test cultures equivalent to 0.5 McFarland standard was used for the light and dark treatment. The bacterial cultures were treated with CNT, TB and TBCNT (50 µg/mL) and the control samples were maintained without any compound. The samples were pre-incubated in dark for 3 h. Two experimental setups were maintained where one was irradiated with light and other kept in dark condition. The irradiated and non-irradiated samples were inoculated in BHI broth having 1% sucrose and incubated for 24 h at 37 °C. After 24 h of incubation, the medium was removed, and the biofilms formed were gently washed with PBS. Fresh medium was supplemented to the wells along with 50 µL of 0.5 mM CR. The plates were incubated for 2 h at room temperature and centrifuged at 10000 rpm for 5 min. EPS was quantified spectrophotometrically by measuring the OD_{490} of the supernatant. The absorbance value of treated sample was subtracted from the blank CR to calculate the amount of EPS produced.

2.11. Confocal laser scanning microscopic analysis (CLSM)

Effect of aPDT on the biofilms when treated with CNT, TB and TBCNT was observed using confocal laser scanning microscopic analysis [35]. Biofilms were provided with growth conditions to establish on sterile coverslips placed in the wells having BHI broth with 1% sucrose. The experimental setup was incubated for 48 h at 37 °C. The biofilms formed were treated with CNT, TB and TBCNT (50 µg/mL) and irradiated for 3 min. Non-irradiated samples were also maintained for comparison. After the treatment both irradiated and non-irradiated samples were washed with sterile PBS to remove planktonic cells. Cells in the biofilm were stained with acridine orange and ethidium bromide at room temperature and left undisturbed for 15 min. Biofilms were visualized using a CLSM (LSM710, Carl Zeiss, Jena, Germany) equipped with argon laser with an excitation wavelength of 488 nm.

2.12. Statistical analysis

All the experiments were conducted in triplicate and represented with their mean and standard deviation. One-way ANOVA was used to analyze the results and the statistically ($P < 0.05$) significant results were represented with asterisk (*) symbol.

3. Results

3.1. Characterization of TBCNT conjugate

The optical properties of CNT, TB and TBCNT were determined using UV–Vis absorption spectroscopy. An intense peak for CNT at 273 nm due to n- π transition in the aromatic ring was observed. The maximum absorbance of TB was observed at 610 nm and a secondary absorption peak at 290 nm. In TBCNT conjugate, peaks observed at 280 and 630 nm were correspond to the absorbance of CNT and TB respectively (Fig. 1A). The quenching in the absorption peaks of TBCNT indicated the binding of TB on to carbon nanotubes. The UV–vis absorption results confirmed the conjugation of cationic dye on CNT. In HRTEM micrograph cylindrical, coiled and branched CNT were observed (Fig. 1B). The infra-red spectra (IR) of CNT, TB and TBCNT were shown in Fig. 2B. The IR spectra of TB showed characteristic vibrations at 1037.2, 1353.4, 1444.1, 1489.2, 1535.7 and 3267.7 cm^{-1}. The functional groups present in CNT were graphed at 1073.6, 1458.3, 1544.8 and 3451.1 cm^{-1}. In CNT, a characteristic oxygen containing band obtained at 3451.1 cm^{-1} corresponds to the O—H stretching vibration and a band at 1073.6 cm^{-1} corresponds to the C—O stretching vibrations of −COOH groups. A sharp peak at 1544 cm^{-1} attributes to the C=C stretching of the benzene ring with C–H bending. The aromatic ring band of TB is observed at 1535.7 cm^{-1} and the band at 3267.1 cm^{-1} depicts N—H stretch due to the primary amine. The characteristic IR spectra of TBCNT conjugate graphed with peaks at

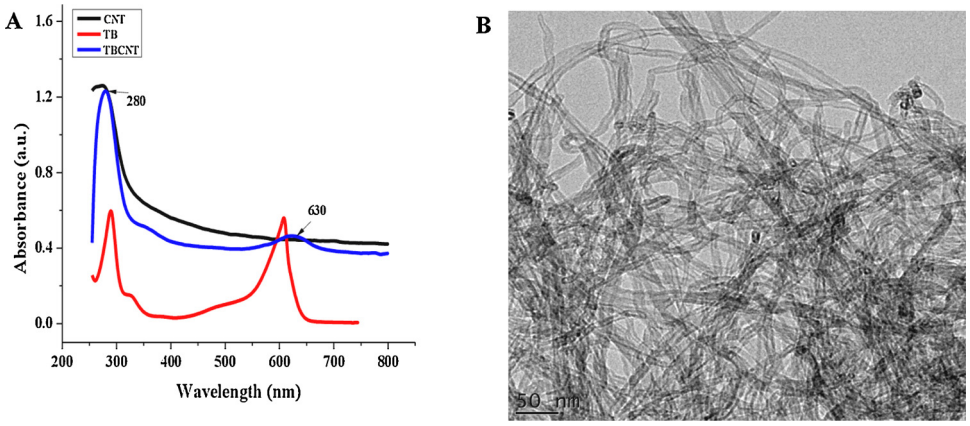

Fig. 1. (A) UV–vis spectroscopic analysis of CNT, TB and TBCNT. CNT and TB exhibited maximum absorbance at 273 and 610 nm respectively. Absorbance bands for TBCNT were recorded at 280 and 630 nm. (B) HRTEM micrograph of TBCNT.

1060.2, 1327.9, 1436.2, 1592.8, 2922.6 and 3442.9 cm^{-1} and represents presence of TB and CNT (Fig. 2A). FTIR spectrum of TBCNT conjugate confirms the conjugation of dye on nanoplatform.

In Raman spectra characteristic peak of TB was observed at 448 cm^{-1}that is associated with the C—N—C skeletal deformation mode (Fig. 2B). Two prominent peaks observed at 1394 and 1623 cm^{-1} attributes to C—N symmetrical stretching and C—C ring stretching respectively. Raman spectra of functionalized CNT showed 2 main first order bands at 1603.1 (G or graphitic band) and 1312.2 cm^{-1} (D or defect band) which corresponds to the vibrations in the planes of the graphene sheets and the defects in the sidewalls of carbon nanotubes respectively. In TBCNT conjugate peaks at 1309.3, 1600, 1760.7, 1853.5, and 1925.5 cm^{-1} correspond to the raman bands of both CNT and toluidine blue. Photoluminescence excitation and emission properties of CNT, TB and TBCNT were studied using fluorescence spectrophotometry. The emission spectra of TB and CNT were recorded at 670 and 375 nm respectively (Fig. 3B and D). The excitation spectra of TB and CNT were observed at 590 and 290 nm (Fig. 3Aand C). The photoluminescence spectrum of TBCNT showed emissions at 657 nm and 361 nm that corresponds to the emission of TB and CNT respectively (Fig. 4A and B). The excitation spectra of TBCNT were graphed at 625 and 273 nm showing TB and CNT excitations respectively (Fig. 4C and D).

3.2. Loading capacity of TB and entrapment efficiency of CNT

Loading and entrapment efficiency are the two important parameters for achieving enhanced phototoxicity against test bacteria. The loading capacity of TB was found to be 12.04 ± 0.55%. The entrapment efficiency of CNT was estimated as 48.99 ± 2.33%.

3.3. Dye release study

In vitro release profile of TB from TBCNT was studied at different time intervals in PBS at room temperature. A continuous release profile of TB was observed with a saturation point at the 180 min (Fig. 5A). The initial release was found to be 19.94 ± 1.61% and which further increased to 98.98 ± 3.34% at 180 min. The release profile shows a complete release of TB from TBCNT at 180 min.

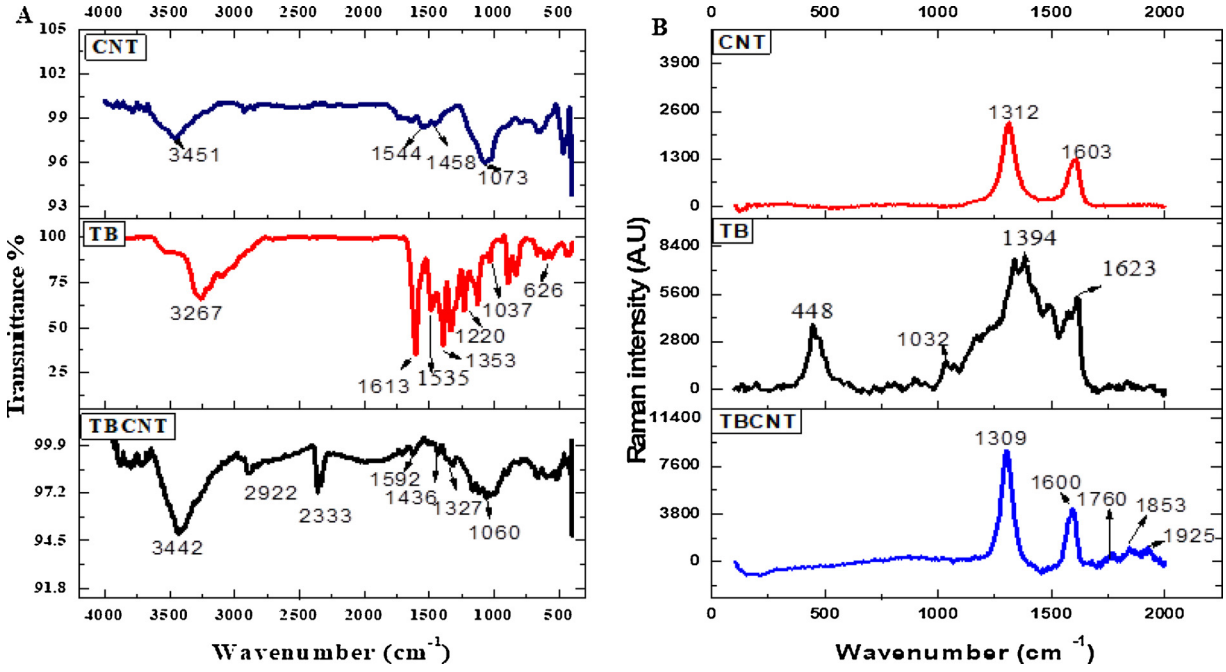

Fig. 2. (A) FTIR spectra of CNT, TB and TBCNT showing characteristic functional groups. (B) Raman spectra of CNT, TB and TBCNT.

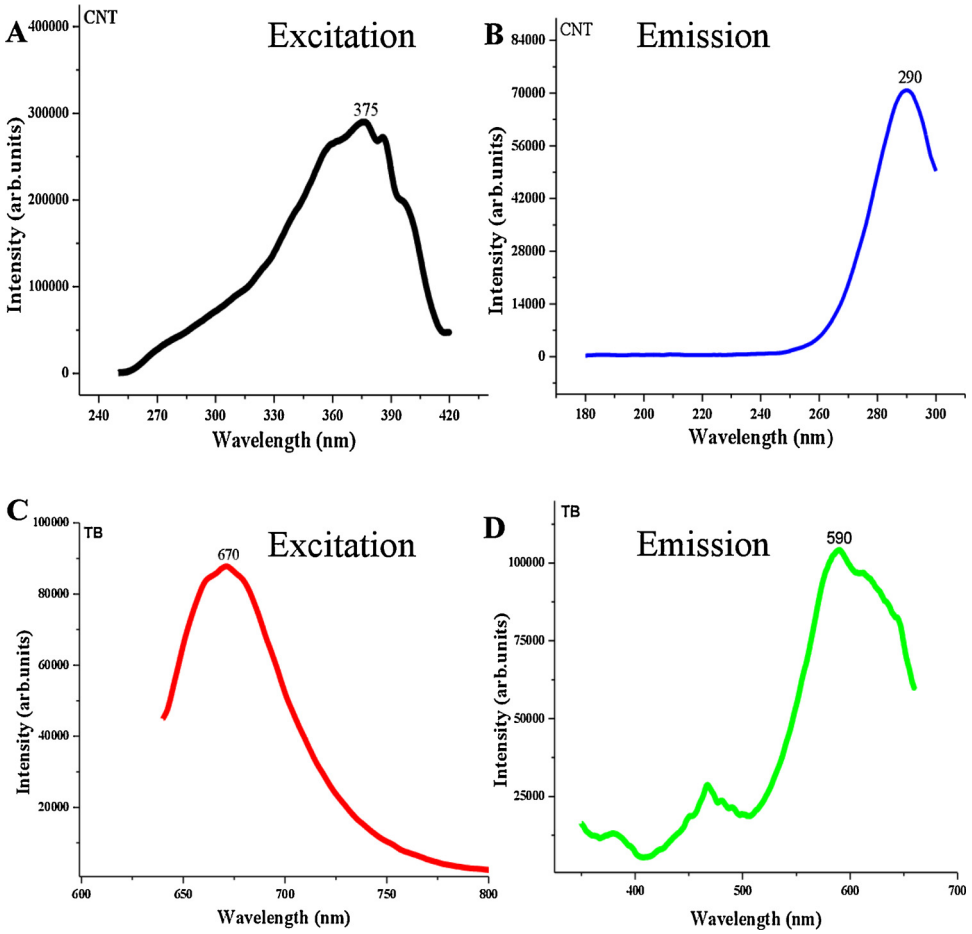

Fig. 3. Photo emission (A) and excitation (B) spectra of CNT. Photo emission (C) and excitation (D) spectra of TB.

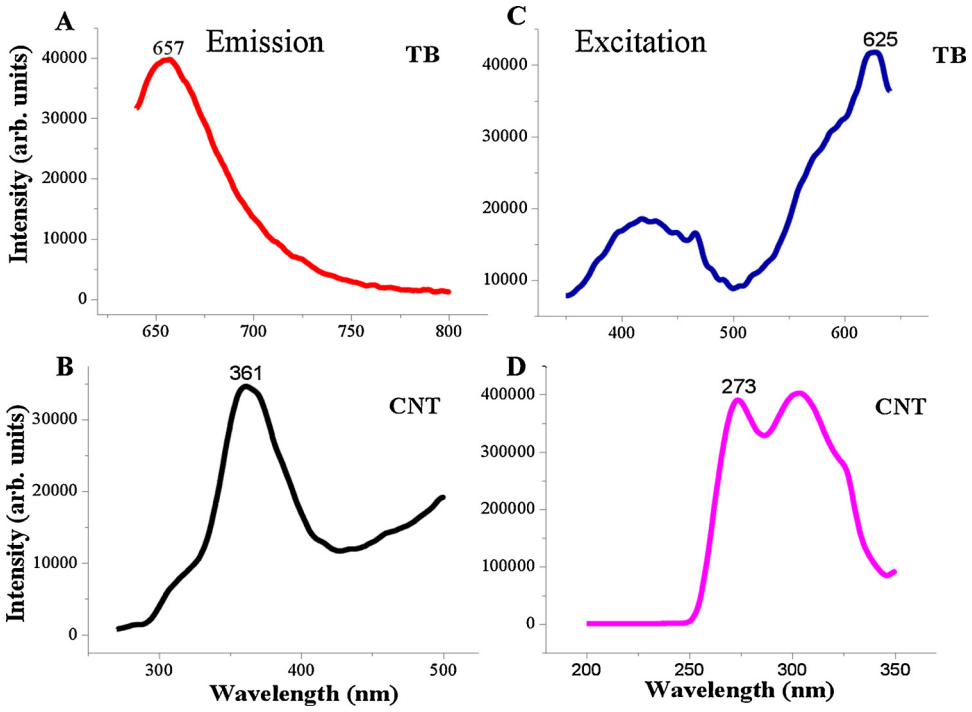

Fig. 4. Photo emission spectra of (A and B) TBCNT. Photo excitation spectra (C and D) of TBCNT.

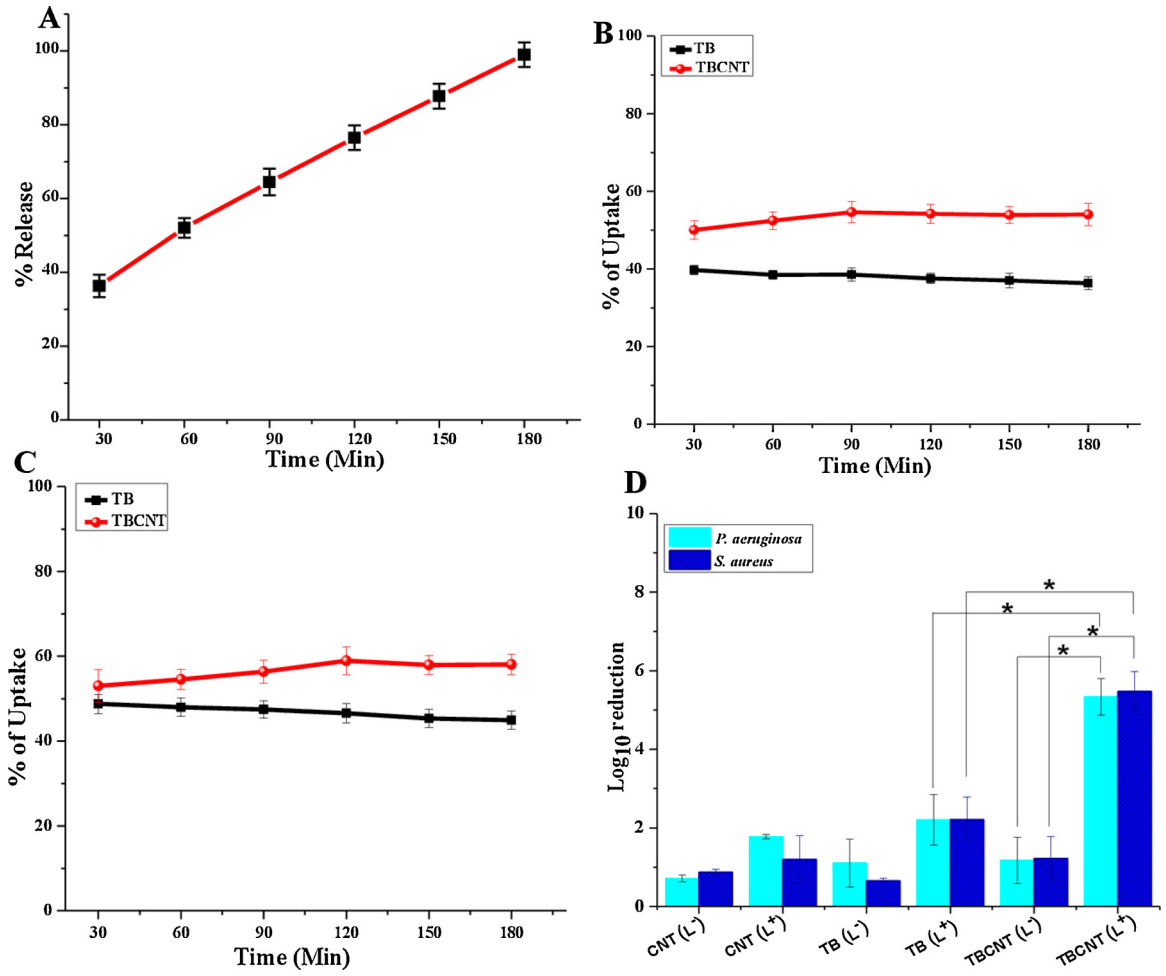

Fig. 5. A) *in vitro* release profile of TB from TBCNT at 37 °C and pH 7.4. Uptake percentages of free TB and TBCNT by test bacteria (B) *P. aeruginosa* PA01 and (C) *S. aureus*. (D) Logarithmic reduction of planktonic cells of *P. aeruginosa* PA01 and *S. aureus* after aPDT (dark (L^-). Non-irradiated and irradiated samples were represented by (L^-) and (L^+). Asterisk (*) represents the statistical significance with respect to the dark control (P value < 0.05).

3.4. Bacterial uptake of TB

The internalization of dye through the bacterial membrane is an important parameter to achieve significant photodynamic inactivation of bacteria. Fig. 5B and C represents the uptake of free dye and TBCNT by *P. aeruginosa* and *S. aureus* at different time intervals. The maximum amount of TB (37.53 ± 1.31%) and TBCNT (54.19 ± 2.43%) uptake was occurred at 120 min in *P. aeruginosa* PA01 (Fig. 5B). The amount of TB uptake from free dye and TBCNT by *S. aureus* was estimated as 46.57 ± 2.26 and 58.96 ± 3.28% respectively at 120 min (Fig. 5C).

3.5. aPDT of planktonic bacteria

The photodynamic destruction of *P. aeruginosa* and *S. aureus* in presence of CNT, TB and TBCNT with a radiant exposure of 58.49 J/cm^2 for 3 min was evaluated. The results were represented as logarithmic reduction in the planktonic cells. The TB and TBCNT treated cells of both the test bacteria showed a significant decrease in planktonic cells. *P. aeruginosa* treated with TBCNT showed 4.91 $\log_{10}$ reduction compared to 2.20 $\log_{10}$ reduction when treated with TB (Fig. 5D). Planktonic cells of *S. aureus* showed a $\log_{10}$ reduction of 5.47 and 2.21 in TBCNT and TB treated samples with light irradiation.

3.6. Study of mechanism of action

3.6.1. Detection of ROS

P. aeruginosa and *S. aureus* treated with TB and TBCNT were observed more DCF fluorescence intensity suggesting higher amount of ROS production. The fluorescence intensity was more in the samples treated with TBCNT compared to the control and non-irradiated samples. A less fluorescence intensity was measured in CNT, TB and TBCNT treated bacteria without irradiation. The fluorescence intensity detected in the irradiated samples was a measure of ROS generated inside the bacteria which influences the cellular damage and photodynamic destruction (Fig. 6A and B).

3.6.2. Cytoplasmic protein leakage

The effect of aPDT on cell membrane was evaluated by measuring the leakage of protein from the cells. The amount of protein leaked in *S. aureus* after treatment with TBCNT and TB was 63.41 ± 1.52 and 21.81 ± 1.14% after light exposure respectively. *P. aeruginosa* showed a protein leakage of 59.19 ± 1.45 and 20.76 ± 0.74% in TBNCT and TB treated samples after irradiation (Fig. 6C). Protein leakage from cells after photoactivation of TBCNT was significantly higher than TB and CNT treated cells. The TBCNT irradiated samples exhibited more protein leakage compared to the non-irradiated samples.

3.6.3. Lipid peroxidation

Lipid peroxides formed after aPDT was measured using MDA

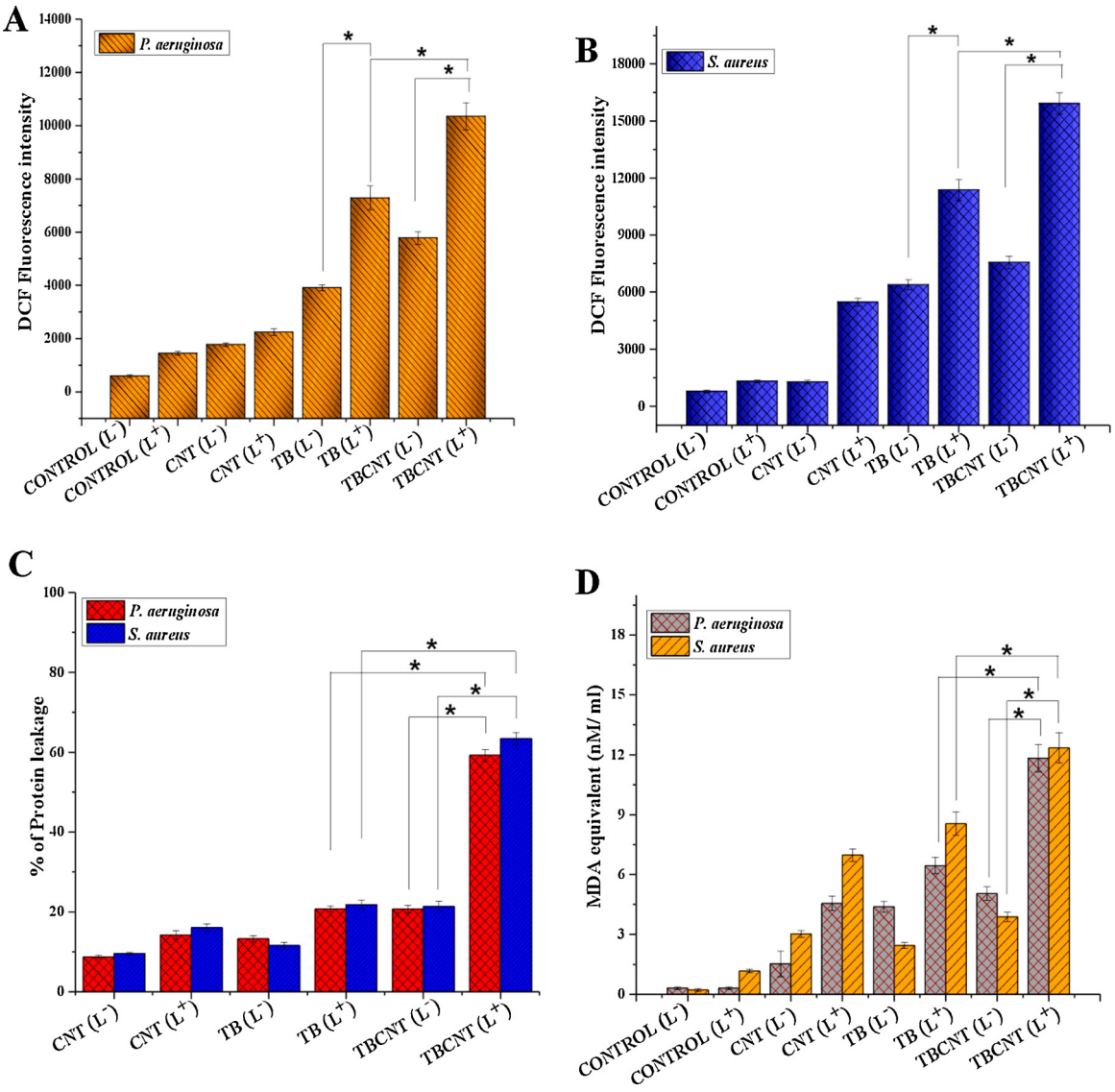

Fig. 6. Total reactive oxygen species detected in (A) *P. aeruginosa* PA01 and (B) *S. aureus* after treatment with CNT, TB, TBCNT in dark and light irradiation. (C) Cytoplasmic protein leakage in *P. aeruginosa* PA01 and *S. aureus* after aPDT. (D) Lipid peroxidation in *P. aeruginosa* PA01 and *S. aureus* after treated with CNT, TB and TBCNT with and without irradiation. Non-irradiated and irradiated samples were represented by (L^-) and (L^+). Asterisk (*) represents the statistical significance with respect to the dark control (P value < 0.05).

standards and found maximum peroxidation in TBCNT treated bacterial cells irradiated with laser. *P. aeruginosa* and *S. aureus* treated with TBCNT after aPDT exhibited a lipid peroxidation of 12.34 ± 0.74 and 11.82 ± 0.68 nM/mL respectively (Fig. 6D). The lipid peroxidation was less in samples treated with TB and TBCNT without light irradiation.

3.7. Antibiofilm activity

3.7.1. Biofilm inhibition

CNT, TB and TBCNT treated bacteria showed higher biofilm inhibition after light irradiation compared to the dark condition. TBCNT conjugate exhibited a significant photodestruction in the biofilm formation after aPDT on the test bacteria. After light irradiation TBCNT conjugate reduced the biofilm formation in *P. aeruginosa* and *S. aureus* by 69.94 ± 2.90 and 74.54 ± 3.77% respectively (Fig. 7A). The formation of biofilms in *P. aeruginosa* and *S. aureus* was inhibited to 34.36 ± 2.90 and 45.22 ± 1.04% in TB treated samples after light irradiation.

3.7.2. Cell viability

The reduction in the viable cells of *P. aeruginosa* PA01 after the treatment with TBCNT and free TB in light irradiation was 56.64 ± 2.15 and 28.82 ± 1.51% respectively (Fig. 7B). TBCNT and TB treated *S. aureus* after light irradiation showed 65.28 ± 2.58 and 33.50 ± 2.01% reduction in cell viability. An enhanced reduction in the cell viability was observed in the samples with light irradiation. Bacteria treated with CNT, TB and TBCNT after irradiation exhibited more reduction in cell viability when compared with non-irradiated samples.

3.7.3. EPS quantification

The effect of aPDT on exopolysaccharide (EPS) production was quantified and a significant reduction was observed in TBCNT treated cells after irradiation. High amount of EPS production was observed in control. EPS production was reduced to 44.51 ± 2.71 and 57.25 ± 3.15% in *P. aeruginosa* and *S. aureus* treated with TBCNT after light irradiation (Fig. 7C). In contrast EPS production was reduced to 24.49 ± 2.16 and 27.11 ± 1.87% in *P. aeruginosa* and *S. aureus* after the treatment with TB.

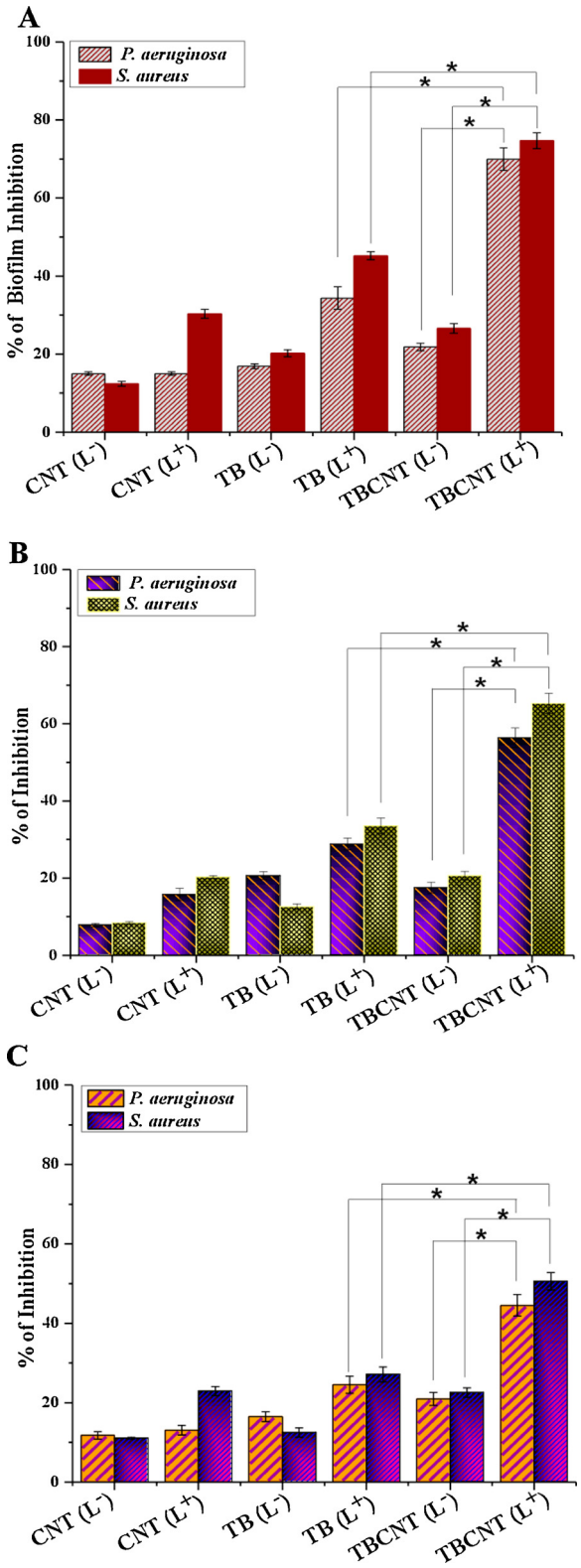

Fig. 7. (A) Biofilm inhibition in *P. aeruginosa* PA01 and *S. aureus* treated with CNT, TB and TBCNT. (B) TTC cell viability assay showing reduction in the viable cells after aPDT with CNT, TB and TBCNT on *P. aeruginosa* PA01 and *S. aureus*. (C) Reduction in the EPS production in *P. aeruginosa* PA01 and *S. aureus* after aPDT in presence of CNT, TB and TBCNT. Non-irradiated and irradiated samples were represented by (L^-) and (L^+). Asterisk (*) represents the statistical significance with respect to the dark control (P value < 0.05).

3.8. CLSM analysis

The effect of aPDT on both bacterial species was visualized using CLSM. Bacterial cells treated with TB and TBCNT with light irradiation showed more-red fluorescence whereas control biofilms showed green fluorescence. The red and green fluorescence corresponds to the dead and live cells after irradiation. The intensity of red-fluorescence was predominant in TBCNT treated biofilms of *P. aeruginosa* PA01 and *S. aureus* after light irradiation (Fig. 8). CLSM images represents photodestrcution of biofilms in the CNT, TB and TBCNT treated bacteria after light irradiation.

4. Discussion

Infections associated with antibiotic resistant bacteria are the primary challenge to public health sector, due to high rates of morbidity and mortality. Multi drug resistant Gram positive and Gram negative bacteria are difficult to treat with conventional antimicrobials [35]. Biofilm forming pathogenic bacteria are responsible for infections such as urinary tract infections (UTI), catheter infections, medical device related infections, middle ear infections, caries and periodontitis. Microbial biofilms are having different properties where self-produced polymeric matrix as surface structure makes them resistant to available antibiotics and antibacterial treatments [36]. These biofilms are characterized by a significant decrease in their antimicrobial susceptibility. For instance, researchers reported that *S. aureus* biofilms require 100 times more MBC concentration of vancomycin for a 3 log reduction in cells [37]. Some of the known nosocomial pathogens responsible for catheter related infections such as *P. aeruginosa* and *S. aureus* establish biofilms on catheter surfaces. These organisms possess various mechanisms of antibiotic resistance and difficulty to prevent [38]. One of the promising alternatives to the currently available antibiotics is antimicrobial photodynamic inactivation. aPDT is a photochemical process where a nontoxic photosensitizer (PS), photo activated in presence of light of appropriate wavelength. The photoactivated PS generates reactive oxygen intermediates which are cytotoxic in nature and damage cellular components [39].

In this context primary focus of this study was to enhance the antibiofilm efficacy of toluidine blue (photosensitizer) by conjugating with multiwalled carbon nanotubes. There are several metal and metal oxide nanoparticles studied for their antimicrobial and antibiofilm properties against broad range of microorganisms [39–41]. Among the carbon nanostructures, carbon nanotubes are having strong antimicrobial activity, suggesting its vast applications in biomedical field. The lethal antibacterial and antibiofilm properties of CNT are highly influenced by their size, diameter, doping, surface functionalization, electronic structure, residual catalyst and surface chemistry [18]. Carbon nanotubes are known to be excellent drug carriers and also possess photo activities. Carbon nanotubes exhibit higher amount of ROS production under UV illumination than other carbon nanostructures like fullerene. Multiwalled carbon nanotubes conjugated with various metallic elements such as TiO_2 and Si exhibited greater phototoxicity against *E. coli* upon illumination with visible light for 60 min [42].

Although the reports regarding the antimicrobial photodynamic inactivation of biofilms using TB are available, photodynamic inactivation of *P. aeruginosa* and *S. aureus* using TBCNT nanoconjugate was not studied. This is the first report on potent antimicrobial and antibiofilm efficacy of photoactivated toluidine blue conjugated carbon nanotubes against *P. aeruginosa* and *S. aureus*. Positively charged dye toluidine blue has significantly inhibited the growth of several Gram negative and positive bacterial pathogens especially oral bacteria. In previous studies, lipopolysaccharides of *E. coli* and proteases of *P. aeruginosa* were photoinactivated in presence of toluidine blue [43].

The prepared nanoconjugate was characterized using UV–vis spectroscopy, FTIR, Raman spectroscopy and photoluminescence

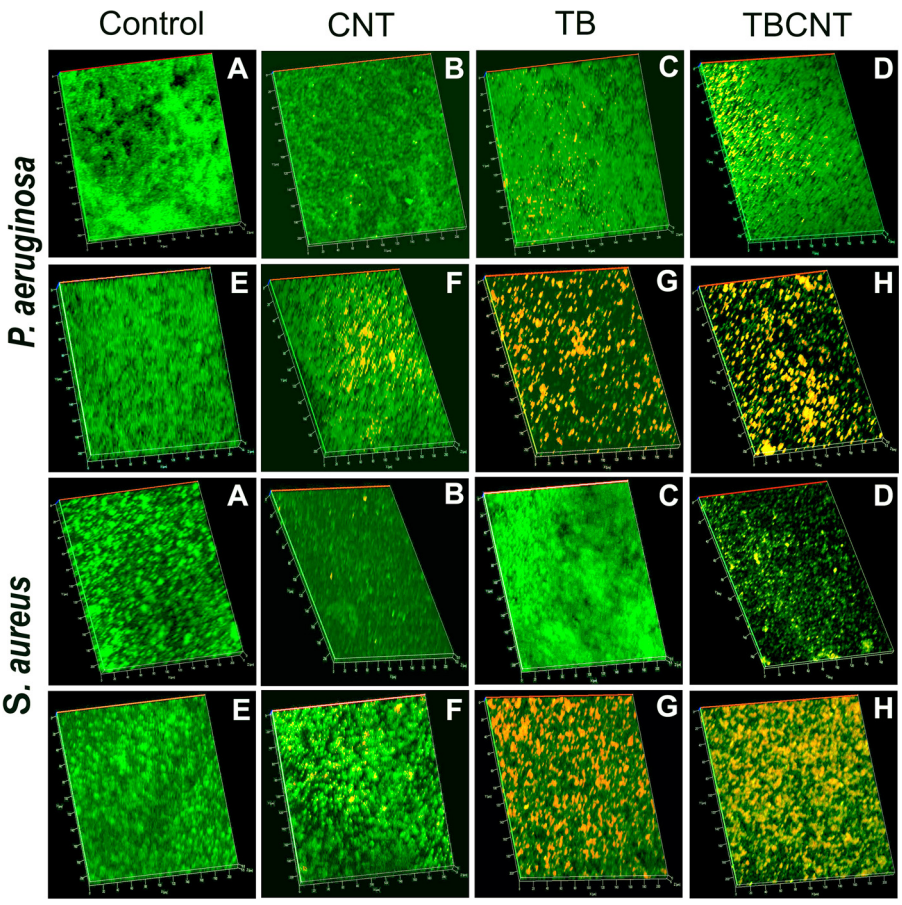

Fig. 8. CLSM analysis of *P. aeruginosa* PA01 and *S. aureus*. (A and E) 3D images of non-irradiated and irradiated (control) biofilms; (B and F) non-irradiated and irradiated biofilms in the presence of CNT; (C and G) non-irradiated and irradiated biofilms in the presence of TB; (D and H) non-irradiated and irradiated biofilms in the presence of TBCNT.

spectroscopy. According to the previous reports CNT and TB showed a maximum absorbance at 280 and 630 nm respectively [44]. Functional group analysis carried out by FTIR spectroscopy depicted the conjugation of dye with carbon nanotubes [45]. The Raman shifts of CNT and TB observed were in agreement with the previous reports [46]. The characterization of TBCNT using various techniques confirmed the conjugation of TB on CNT.

Loading capacity of dye and entrapment efficiency of CNT are two important parameters in antimicrobial photodynamic inactivation. The efficiency of photodynamic destruction varies according to the photosensitizer properties including the amount of energy needed to activate the PS, penetration depth of laser, the charge and purity of the PS molecule, specificity of PS for the bacteria, time of illumination and the uptake kinetics. The loading and encapsulation efficiency of TB was measured as 12.04 ± 0.55% and 48.99 ± 2.33, where as in Usacheva et al., 2016 has reported the loading of TB in alginate nanoparticles as 10.8 ± 2.2% [27]. Moreover TBCNT conjugate was observed with maximum release of dye at 180 min when compared to other nano-dye conjugate. The release of TB from a carbomer hydrogel was reported as 68.26% in 24 h [23]. The release profile of TB from TBCNT showed a sustained and controlled release (98.98 ± 3.34%) with a saturation point after 180 min. Uptake of TB- alginate nanoparticle and free TB by *P. aeruginosa* was reported as 39.4 and 22.7% respectively [27]. Binding efficiency of dye to the bacterial cells differs based on the physiology of bacterial membrane and charge of dye molecules. In this work, TBCNT uptake was recorded as 54.19 ± 2.43 and 58.96 ± 3.28% in *P. aeruginosa* and *S. aureus* bacterial system respectively which lead to the effective photodynamic destruction of bacteria. The high uptake of dye from TBCNT conjugate over free dye has indicated the advantage of using nanoplatform in this work for the effective antimicrobial photodynamic inactivation of test bacteria.

The TBCNT conjugate synthesized in this work is having the following beneficial characteristics: (i) The TBCNT conjugate synthesized is an effective broad spectrum antibacterial agent; (ii) TB exerted phototoxic effect on both the test bacteria, *P. aeruginosa* PA01 and *S. aureus* (iii) The conjugation of dye onto CNT results in the effective delivery of PS to the biofilms and enhanced activity [22]. The photoinactivation of TBCNT conjugate on planktonic cells and biofilms of *P. aeruginosa* PA01 and *S. aureus* was observed more when compared to previous reports. Previous studies on aPDT using chitosan-TB reported a 4 log reduction of *S. aureus* and *P. aeruginosa* with a radiant exposure of 20 J/cm ^{2} [47]. In another study on photodynamic therapy, oral microorganisms in their planktonic stage were significantly reduced to 3.06 $\log_{10}$ CFU/mL when treated with toluidine blue (100 µg/mL) with an exposure time of 5 min. In the same study, they have found that biofilms of oral bacteria were significantly reduced to 2.21 $\log_{10}$ [48]. The present study showed a 4.91 and 5.47 $\log_{10}$ reductions of *P. aeruginosa* PA01 and *S. aureus* respectively with a radiant exposure of 58.49 J/ cm^2.

The mechanism of action of aPDT on both the bacterial species was studied through cytoplasmic leakage and lipid peroxidation activities. The ROS generated after aPDT was responsible for the altered cell membrane integrity which leads to cellular damage [49]. Light activated PS generates ROS which causes the oxidation of certain vital biomolecules, leakage of cytoplasmic contents and lipid peroxidation [49,50]. The antibacterial activity of nanoconjugate can be enhanced more by reducing the dimension of carbon nanotubes. Previous studies showed that CNT with shorter length are having increased surface area which aids in the enhanced interaction and uptake by bacteria. The biological effects exhibited by shorter CNTs will be improved compared to the larger form [17]. In future, antimicrobial photodynamic activity of TBCNT conjugate can be improved by reducing the dimension of carbon nanotubes.

TBCNT conjugate prepared in this study exhibited significant

photodestruction on planktonic cells and biofilms of test bacteria. The photodynamic therapy using TBCNT conjugate can be used as an alternative approach to the conventional methods in the treatment of localized infections and the infections associated with medical devices.

5. Conclusion

Nanotechnology has grazed upon several fields of biology and medicine. Particles in their nanosize have gained more attention in antimicrobial therapy as drug carriers. Carbon nanotubes are known as attractive scaffolds for the targeted delivery of drug with improved efficacy. In this work CNT is used as a dye delivery vehicle to the bacterial cells which enhances the antimicrobial photodynamic inactivation of bacteria. This is the first report on TBCNT conjugate for photodynamic inactivation. The present study provides insights into the synthesis and mechanism of antimicrobial activity of TBCNT conjugate after light illumination. The toluidine blue conjugated carbon nanotube was successfully used for the reduction and eradication of both the planktonic cells and biofilms of *P. aeruginosa* and *S. aureus*. The novel conjugate can be used as an effective antimicrobial agent to treat drug resistant and biofilm forming bacteria.

Declaration of Competing Interest

The authors report no conflicts of interest in this work.

Acknowledgements

The authors are thankful to Central Instrumentation Facility (CIF) of Pondicherry University, Department of Physics (Pondicherry University) and iThemba LABS-National Research Foundation (NRF), Somerset West, Western Cape Province, South Africa for providing various instrumentation facilities. The authors also would like to extend their sincere appreciation to King Saud University, Deanship of Scientific Research, College of Sciences, Research Centre for its supporting of this research. Authors are thankful to Bharathidasan University, Tiruchirappalli for providing the Confocal Laser Scanning Microscopy facility.

References

[1] P. Rai, S. Mallidi, X. Zheng, R. Rahmanzadeh, Y. Mir, S. Elrington, A. Khurshid, T. Hasan, Development and applications of photo-triggered theranostic agents, Adv. Drug Deliv. Rev. 62 (2010) 1094–1124, https://doi.org/10.1016/j.addr.2010.09.002.

[2] S. Miquel, R. Lagrafeuille, B. Souweine, C. Forestier, Anti-biofilm activity as a health issue, Front. Microbiol. 7 (2016) 1–14, https://doi.org/10.3389/fmicb.2016.00592.

[3] M. Frieri, K. Kumar, A. Boutin, Antibiotic resistance, J. Infect. Public Health 10 (2017) 369–378, https://doi.org/10.1016/j.jiph.2016.08.007.

[4] D. Lebeaux, J.-M. Ghigo, C. Beloin, Biofilm-related infections: bridging the gap between clinical management and fundamental aspects of recalcitrance toward antibiotics, Microbiol. Mol. Biol. Rev. 78 (2014) 510–543, https://doi.org/10.1128/MMBR.00013-14.

[5] A. Taraszkiewicz, G. Fila, M. Grinholc, J. Nakonieczna, Innovative strategies to overcome biofilm resistance, Biomed Res. Int. 2013 (2013) 1–13, https://doi.org/10.1155/2013/150653.

[6] L. Huang, Y. Xuan, Y. Koide, T. Zhiyentayev, M. Tanaka, M.R. Hamblin, Type I and Type II mechanisms of antimicrobial photodynamic therapy: an in vitro study on gram-negative and gram-positive bacteria, Lasers Surg. Med. 44 (2012) 490–499, https://doi.org/10.1002/lsm.22045.

[7] Z. Oruba, P. Łabuz, W. Macyk, M. Chomyszyn-Gajewska, Antimicrobial photodynamic therapy-A discovery originating from the pre-antibiotic era in a novel periodontal therapy, Photodiagnosis Photodyn. Ther. 12 (2015) 612–618, https://doi.org/10.1016/j.pdpdt.2015.10.007.

[8] Merrill A. Biel, Chet Sievert, Marina Usacheva, Eric Wedell, Nicolas Loebel, Andreas Rose, R. Zimmermann, Reduction of endotracheal tube biofilms using antimicrobial photodynamic therapy, Lasers Surg. Med. 43 (2012) 586–590, https://doi.org/10.1002/lsm.21103.

[9] O.S. Adeyemi, F.A. Sulaiman, Evaluation of metal nanoparticles for drug delivery systems, J. Biomed. Res. 29 (2015) 145–149, https://doi.org/10.7555/JBR.28.20130096.

[10] G. Franci, A. Falanga, S. Galdiero, L. Palomba, M. Rai, G. Morelli, M. Galdiero, Silver nanoparticles as potential antibacterial agents, Molecules. 20 (2015) 8856–8874, https://doi.org/10.3390/molecules20058856.

[11] C. Maria Magdalane, J. Kennedy, S. Jasmine Shahina, M. Maaza, R. Sundaram, A. Mobeen Amanulla, S.B. Mohamed, K. Kaviyarasu, D. Letsholathebe, Antibacterial, magnetic, optical and humidity sensor studies of β-CoMoO 4 - Co 3 O 4 nanocomposites and its synthesis and characterization, J. Photochem. Photobiol. B, Biol. 183 (2018) 233–241, https://doi.org/10.1016/j.jphotobiol.2018.04.034.

[12] K. Kaviyarasu, N. Geetha, K. Kanimozhi, C. Maria Magdalane, S. Sivaranjani, A. Ayeshamariam, J. Kennedy, M. Maaza, In vitro cytotoxicity effect and antibacterial performance of human lung epithelial cells A549 activity of Zinc oxide doped TiO 2 nanocrystals: investigation of bio-medical application by chemical method, Mater. Sci. Eng. C. 74 (2017) 325–333, https://doi.org/10.1016/j.msec.2016.12.024.

[13] A. Angel Ezhilarasi, J. Judith Vijaya, K. Kaviyarasu, L. John Kennedy, R.J. Ramalingam, H.A. Al-Lohedan, Green synthesis of NiO nanoparticles using Aegle marmelos leaf extract for the evaluation of in-vitro cytotoxicity, antibacterial and photocatalytic properties, J. Photochem. Photobiol. B, Biol. 180 (2018) 39–50, https://doi.org/10.1016/j.jphotobiol.2018.01.023.

[14] D. Saravanakkumar, S. Sivaranjani, K. Kaviyarasu, A. Ayeshamariam, B. Ravikumar, S. Pandiarajan, C. Veeralakshmi, M. Jayachandran, M. Maaza, Synthesis and characterization of ZnO–CuO nanocomposites powder by modified perfume spray pyrolysis method and its antimicrobial investigation, J. Semicond. 39 (2018) 033001, , https://doi.org/10.1088/1674-4926/39/3/033001.

[15] M.R. Saboktakin, R.M. Tabatabaee, The novel polymeric systems for photodynamic therapy technique, Int. J. Biol. Macromol. 65 (2014) 398–414, https://doi.org/10.1016/j.ijbiomac.2014.01.019.

[16] A. Eatemadi, H. Daraee, H. Karimkhanloo, M. Kouhi, N. Zarghami, A. Akbarzadeh, M. Abasi, Y. Hanifehpour, S. Joo, Carbon nanotubes: properties, synthesis, purification, and medical applications, Nanoscale Res. Lett. 9 (2014) 393, https://doi.org/10.1186/1556-276X-9-393.

[17] S. Kang, M. Herzberg, D.F. Rodrigues, M. Elimelech, Antibacterial Effects of Carbon Nanotubes: Size Does Matter!, Langmuir 24 (2008) 6409–6413, https://doi.org/10.1021/la800951v.

[18] A. Al-Jumaili, S. Alancherry, K. Bazaka, M. Jacob, Review on the antimicrobial properties of carbon nanostructures, Materials (Basel). 10 (2017) 1066, https://doi.org/10.3390/ma10091066.

[19] T. Mocan, C.T. Matea, T. Pop, O. Mosteanu, A. Dana, S. Suciu, C. Puia, C. Zdrehus, C. Iancu, L. Mocan, Carbon nanotubes as anti-bacterial agents, Cell. Mol. Life Sci. 74 (2017) 3467–3479, https://doi.org/10.1007/s00018-017-2532-y.

[20] A.B. Ormond, H.S. Freeman, Dye sensitizers for photodynamic therapy, Materials (Basel). (2013) 817–840, https://doi.org/10.3390/ma6030817.

[21] H. Kariminezhad, H. Amani, Photodynamic inactivation of E. coli PTCC 1276 using light emitting diodes: Application of rose Bengal and methylene blue as two simple models, (2017), pp. 967–977, https://doi.org/10.1007/s12010-016-2374-3.

[22] L. Misba, S. Kulshrestha, A.U. Khan, Antibiofilm action of a toluidine blue O-silver nanoparticle conjugate on *Streptococcus mutans* : a mechanism of type I photodynamic therapy, Biofouling 32 (2016) 313–328, https://doi.org/10.1080/08927014.2016.1141899.

[23] H. Liang, J. Xu, Y. Liu, J. Zhang, W. Peng, J. Yan, Z. Li, Q. Li, Optimization of hydrogel containing toluidine blue O for photodynamic therapy by response surface methodology, J. Photochem. Photobiol. B, Biol. 173 (2017) 389–396, https://doi.org/10.1016/j.jphotobiol.2017.06.019.

[24] U. Sah, K. Sharma, N. Chaudhri, M. Sankar, P. Gopinath, Antimicrobial photodynamic therapy: single-walled carbon nanotube (SWCNT)-Porphyrin conjugate for visible light mediated inactivation of Staphylococcus aureus, Colloids Surf. B Biointerfaces 162 (2018) 108–117, https://doi.org/10.1016/j.colsurfb.2017.11.046.

[25] Z. Mai, J. Chen, Y. Hu, F. Liu, B. Fu, H. Zhang, X. Dong, W. Huang, W. Zhou, Novel functional mesoporous silica nanoparticles loaded with vitamin E acetate as smart platforms for pH responsive delivery with high bioactivity, J. Colloid Interface Sci. 508 (2017) 184–195, https://doi.org/10.1016/j.jcis.2017.07.027.

[26] K.D. Wani, B.S. Kadu, P. Mansara, P. Gupta, A.V. Deore, R.C. Chikate, P. Poddar, S.D. Dhole, R. Kaul-Ghanekar, Synthesis, characterization and in vitro study of biocompatible cinnamaldehyde functionalized magnetite nanoparticles (CPGF Nps) for hyperthermia and drug delivery applications in breast cancer, PLoS One 9 (2014) e107315, , https://doi.org/10.1371/journal.pone.0107315.

[27] M. Usacheva, B. Layek, S.S.R. Nirzhor, S. Prabha, Nanoparticle-mediated photodynamic therapy for mixed biofilms, Hindawi 2016 (2016) doi:/10.1155/2016/4752894.

[28] A. VT, P. Paramanantham, S.L. SB, A. Sharan, M.H. Alsaedi, T.M.S. Dawoud, S. Asad, S. Busi, Antimicrobial photodynamic activity of rose Bengal conjugated multi walled carbon nanotubes against planktonic cells and biofilm of *Escherichia coli*, Photodiagnosis Photodyn. Ther. 24 (2018) 300–310, https://doi.org/10.1016/j.pdpdt.2018.10.013.

[29] T.W. Wong, E.C. Wu, W.C. Ko, C.C. Lee, L.I. Hor, I.H. Huang, Photodynamic inactivation of methicillin-resistant *Staphylococcus aureus* by indocyanine green and near infrared light, Dermatologica Sin. 36 (2018) 8–15, https://doi.org/10.1016/j.dsi.2017.08.003.

[30] Q.Z. Zhang, K.Q. Zhao, Y. Wu, X.H. Li, C. Yang, L.M. Guo, C.H. Liu, D. Qu, C.Q. Zheng, 5-aminolevulinic acid-mediated photodynamic therapy and its strain-dependent combined effect with antibiotics on *Staphylococcus aureus* biofilm, PLoS One 12 (2017), https://doi.org/10.1371/journal.pone.0174627.

[31] S. Qayyum, M. Oves, A.U. Khan, Obliteration of bacterial growth and biofilm through ROS generation by facilely synthesized green silver nanoparticles, PLOS. (2017) 1–18, https://doi.org/10.1371/journal pone.0181353.

[32] M. Eshed, J. Lellouche, A. Gedanken, E. Banin, A Zn-Doped CuO nanocomposite

shows enhanced antibiofilm and antibacterial activities against *Streptococcus mutans* compared to nanosized CuO, Adv. Funct. Mater. 24 (2014) 1382–1390, https://doi.org/10.1002/adfm.201302425.
[33] J. Kwiecinska-piróg, T. Bogiel, K. Skowron, E. Wieckowska, E. Gospodarek, Proteus mirabilis biofilm - Qualitative and quantitative colorimetric methods-based evaluation, Braz. J. Microbiol. 1421 (2014) 1415–1421.
[34] L. Misba, S. Zaidi, A.U. Khan, Photodiagnosis and photodynamic therapy A comparison of antibacterial and antibiofilm efficacy of phenothiazinium dyes between gram positive and gram negative bacterial biofilm, Photodiagnosis Photodyn. Ther. 18 (2017) 24–33, https://doi.org/10.1016/j.pdpdt.2017.01.177.
[35] S. Schastak, S. Ziganshyna, B. Gitter, P. Wiedemann, T. Claudepierre, Efficient photodynamic therapy against gram-positive and gram-negative bacteria using THPTS, a cationic photosensitizer excited by infrared wavelength, PLoS One 5 (2010) e11674, , https://doi.org/10.1371/journal.pone.0011674.
[36] W.C.M.A. de Melo, P. Avci, M.N. de Oliveira, A. Gupta, D. Vecchio, M. Sadasivam, R. Chandran, Y.-Y. Huang, R. Yin, L.R. Perussi, G.P. Tegos, J.R. Perussi, T. Dai, M.R. Hamblin, Photodynamic inactivation of biofilm: taking a lightly colored approach to stubborn infection, Expert Rev. Anti. Ther. 11 (2013) 669–693, https://doi.org/10.1586/14787210.2013.811861.
[37] M.J. Franklin, C. Chang, T. Akiyama, B. Bothner, New technologies for studying biofilms, Microbiol. Spectr. 3 (2015) 801–810, https://doi.org/10.1128/microbiolspec.MB-0016-2014.
[38] E. Kalaiarasan, K. Thirumalaswamy, B.N. Harish, V. Gnanasambandam, V.K. Sali, J. John, Inhibition of quorum sensing-controlled biofilm formation in *Pseudomonas aeruginosa* by quorum-sensing inhibitors, Microb. Pathog. 111 (2017) 99–107, https://doi.org/10.1016/j.micpath.2017.08.017.
[39] R. Malik, A. Manocha, D.K. Suresh, Photodynamic therapy - a strategic review, Indian J. Dent. Res. 21 (2010) 285, https://doi.org/10.4103/0970-9290.66659.
[40] S. Valsalam, P. Agastian, M.V. Arasu, N.A. Al-Dhabi, A.-K.M. Ghilan, K. Kaviyarasu, B. Ravindran, S.W. Chang, S. Arokiyaraj, Rapid biosynthesis and characterization of silver nanoparticles from the leaf extract of *Tropaeolum majus* L. and its enhanced in-vitro antibacterial, antifungal, antioxidant and anticancer properties, J. Photochem. Photobiol. B, Biol. 191 (2019) 65–74, https://doi.org/10.1016/j.jphotobiol.2018.12.010.
[41] S.M. Hoseini-Alfatemi, A. Karimi, S. Armin, S. Fakharzadeh, F. Fallah, S. Kalanaky, Antibacterial and antibiofilm activity of nanochelating based silver nanoparticles against several nosocomial pathogens, Appl. Organomet. Chem. 32 (2018) e4327, https://doi.org/10.1002/aoc.4327.
[42] O. Akhavan, M. Abdolahad, Y. Abdi, S. Mohajerzadeh, Synthesis of titania/carbon nanotube heterojunction arrays for photoinactivation of *E. coli* in visible light irradiation, Carbon 47 (2009) 3280–3287, https://doi.org/10.1016/j.carbon.2009.07.046.
[43] M.R. Hamblin, T. Hasan, Photodynamic therapy: a new antimicrobial approach to infectious disease? Photochem. Photobiol. Sci. 3 (2004) 436, https://doi.org/10.1039/b311900a.
[44] H. Kitching, a J. Kenyon, I.P. Parkin, The interaction of gold and silver nanoparticles with a range of anionic and cationic dyes, Phys. Chem. Chem. Phys. 16 (2014) 6050–6059, https://doi.org/10.1039/c3cp55366c.
[45] B. Ganguly, R.K. Nath, A.K. Panda, Spectral studies on the interaction of toluidine blue O with bovine serum albumin, J SurfaceSci. Technol. 29 (2013) 1–16.
[46] R. Mažeikienė, G. Niaura, O. Eicher-Lorka, A. Malinauskas, Raman spectro-electrochemical study of Toluidine Blue, adsorbed and electropolymerized at a gold electrode, Vib. Spectrosc. 47 (2008) 105–112, https://doi.org/10.1016/j.vibspec.2008.02.018.
[47] T. Tsai, H.F. Chien, T.H. Wang, C.T. Huang, Y.B. Ker, C.T. Chen, Chitosan augments photodynamic inactivation of gram-positive and gram-negative bacteria, Antimicrob. Agents Chemother. 55 (2011) 1883–1890, https://doi.org/10.1128/AAC.00550-10.
[48] A. Al-Ahmad, M. Bucher, A.C. Anderson, C. Tennert, E. Hellwig, A. Wittmer, K. Vach, L. Karygianni, Antimicrobial photoinactivation using visible light plus water-filtered Infrared-A (VIS + wIRA) alters in situ oral biofilms, PLoS One 10 (2015) e0132107, , https://doi.org/10.1371/journal.pone.0132107.
[49] M. Grinholc, J. Nakonieczna, G. Fila, Antimicrobial photodynamic therapy with fulleropyrrolidine: photoinactivation mechanism of *Staphylococcus aureus*, in vitro and in vivo studies, Appl. Microbiol. Biotechnol. (2015) 4031–4043, https://doi.org/10.1007/s00253-015-6539-8.
[50] K. Nakamura, Y. Yamada, H. Ikai, T. Kanno, K. Sasaki, Y. Niwano, Bactericidal action of photoirradiated gallic acid via reactive oxygen species formation, J. Agric. Food Chem. 60 (2012) 10048–10054, https://doi.org/10.1021/jf303177p.